An Iris Recognition System Based on Angular Radial Partitioning and Statistical Texture Analysis with Sum & Difference Histogram

Abbas Memiş
Department of Computer Engineering
Yıldız Technical University
İstanbul, Turkey
abbasmemis@gmail.com

Songül Albayrak
Department of Computer Engineering
Yıldız Technical University
İstanbul, Turkey
songul@ce.yildiz.edu.tr

Elena Battini Sönmez
Department of Computer Engineering
İstanbul Bilgi University
İstanbul, Turkey
elena.sonmez@bilgi.edu.tr

***Abstract*—Iris based identification systems are considered among the most promising recognition systems due to the inner characteristics of the iris, such as uniqueness, stability and time invariance. This paper proposes a new texture based iris recognition system based on Angular Radial Partitioning (ARP) and Sum & Difference Histogram (SDH). After the iris segmentation step, ARP is used to divide the iris's texture into sectors, SDH allows for the production of probability vectors, which are then used to extract statistical features. Finally, classification is performed with the K-Nearest Neighbour algorithm. Experimental results on the Ubiris and Upol databases testify the superior performance of the proposed approach, which can handle the presence of eyelids and eyelashes, as well as partially occluded irises and out of focus images. In all experiments the accuracy of the our system is around 97% also when the training set is made up of only two pictures per class, and the corresponding low percentage of FAR suggests that the proposed approach is a good prototype for biometric recognition systems run in identification mode.**

***Keywords*—Iris recognition, Angular Radial Partitioning (ARP), texture analysis, Sum & Difference Histogram (SDH).**

I. Introduction

Recent call for better security together with the rapid progress in electronic and Internet use, have brought biometrics based personal identification systems into focus. Biometrics is the science to identify a person by his/her inner characteristics, which include (but are not limited to) a person's fingerprint, palm print, face, iris, voice, gait or signature. Biometrics based systems are consider more reliable than the traditional ones, based on identification cards, personal numbers and passwords, because inner attributes cannot be lost, forgotten or shared.

The human iris is the annular and colourful part of the eye between the black pupil and the white sclera. The iris pattern contains many distinctive features such as pigment spots, freckles, stripes, furrows, coronas etc., which are located randomly at gestation time. Together with this unique aspect, the iris has the advantages (1) to be an internal and well protected organ of the eye, (2) to be a planar object, insensitive to illumination effects, and (3) to be time invariant. However, current iris-based recognition systems are severely limited by low robustness, accuracy and speed of the algorithms when dealing with poor quality images, which have been acquired in presence of motion, partial cooperation and distance from the camera.

In this paper we propose a new texture-based iris recognition system, which as the advantage to be robust to a large variety of disturbance elements, such as partial occlusion of the iris, presence of eyelashes on the iris's texture, poor focus of the image, and presence of reflection of the camera. Moreover, we detailed our experiments so as to make it reproducible and to allow for comparison with other iris recognition systems.

The first iris-based recognition system was proposed by Daugman, [1] [2] [3], who segmented the iris region with an integro-differential operator and encoded the iris feature by 2D Wavelets demodulation, which resulted in 2048 bits of phase information. The percentage of mismatched bits is calculated with an XOR operator and the Hamming distance gives the difference between any pair of iris codes. Wildes' system [4] generated iris code using a Laplacian pyramid with four different resolution levels; resulting features were down-sampled with Fisher's linear discriminant [5] and compared via normalized correlation. Boles and Bonashash [6] extracted the iris features from the zero-crossing representation of a concentric circle of an iris image using one-dimensional wavelet transform at various resolution levels; classification is performed using two dissimilarity functions. Ma et al. [7] decomposed the iris texture into a set of one-dimensional (1D) intensity signals; the obtained iris features are down-sampled with Fisher linear discriminant [5] and classification is based on cosine similarity. Bowyer et al. [8] presented a comprehensive survey on iris biometrics, which summarizes the state of art up to 2008. In 2009, Chen and Chu [9] extracted the iris feature using a Sobel operator and 1-D wavelet transform and made classification with a mixture of probabilistic neural network (PNN) and particle swarm optimization (PSO). In 2011, Sibai et al. [10] performed iris recognition with neural networks, while Pillai et al. [11] used random projection and sparse representation. At current time, iris based recognition systems are still considered as one of the most promising biometric identification technique, and there is big research effort to increase robustness, accuracy and speed of these algorithms in case of problematic pictures. Among the others, Si et al. [12] proposed (1) a new eyelashes detection algorithm, (2) the use of a 2-D filter for feature extraction and (3) a corner based iris identification method to speed up the 1:N search in big irises databases; while Rahulkar and Holambe [13] presented a shift, scale and rotation invariant

technique for iris feature extraction.

In the proposed iris recognition system (1) the iris region is segmented using a variation of the Daugman's integro-differential operator, (2) each isolated iris pattern is then partitioned into sectors with the Angular Radial Partitioning (ARP) method [14], (3) the Sum & Difference Histogram (SDH) technique [15] is used to represent every sector with a couple of fix sized vectors, (4) which are then converted into a set of statistical features. Finally, (5) classification is performed via the K-Nearest Neighbour method using the Manhattan distance.

We worked with the Ubiris and Upol databases, which are common used databases having a wide variety of disturbance elements, such as occluded irises, poor focus of the images, illumination effects, and blurred edges. We compared our results with the ones of similar experiments run by Celebi [16] and Erbilek and Toygar [17].

To summarize, the main contribution of this work are (1) the introduction of a new, promising, texture-based iris recognition system and (2) the detailed description of the experiments, so as to make them reproducible and allow for comparison with other methods.

Section II describes the segmentation step, which includes the isolation of the iris from the rest of the eye and the subdivision of the iris texture into segments. Section III illustrates the feature extraction process, with the Sum & Difference Histograms technique followed by the extraction of statistical features from texture. Section IV details the experiments run on the Ubiris and Upol databases and compares our results against the ones present in the literature. Conclusions are drawn in Section V.

II. Segmentation

A. Iris Segmentation

The first step in all iris recognition algorithms is to find both the inside (papillary) and the outside (limbus) boundaries of the iris. Different methods have been applied such as the Daugman's integro-differential operator, [1], [2], [3], and the Canny's edge detection with circular Hough Transform [18].

Equation 1 gives the formula of the integro-differential operator of Daugman:

$$max(r, x_0, y_0) \left| G_\sigma(r) * \frac{\partial}{\partial r} \oint_{r,x_0,y_0} \frac{I(x,y)}{2\pi r} ds \right| \qquad (1)$$

where $I(x,y)$ is the input image containing the eye, (x_0, y_0) is the centre of a circular arc ds of radius r, and $G_\sigma(r)$ is a Gaussian smoothing function. The operator defined in (1) is a circular edge detector that must be applied two times to detect the papillary and the limbus boundaries, since they are, generally, not concentric; that is, it is necessary to search for the three parameters (x_0, y_0, r) of the two circles separately. The final result of these operations is the isolation of the iris from the rest of the eye.

Most of the present iris-recognition algorithms are sensitive to the outputs of the iris-segmentation step, where the disturbances caused by an inaccurate detection of inner and outer boundaries are generally removed by ignoring the borders areas. Among the other, this problem was faced by (1) Jang et al. in [19] who proposed a new solution to detect and localize eyelids; (2) Tan et al. in [20] who focused on efficient and robust segmentation of iris images; but, in the recent work of Si et al., [12], it is pointed out that still there is not a feasible solution for the presence of eyelashes.

We applied two different variations of the Daugman's integro-differential operator, one for each of the two databases used.

On the Ubiris [21] database, we decreased the effect of the presence of eyelids and eyelashes by restricting the original image domain and considering only some angles, (θ_1, θ_2), as illustrated in figure 1:

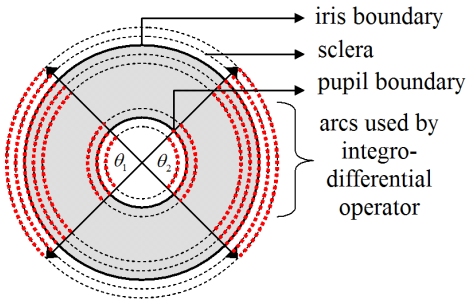

Fig. 1. Arc gradient model used in equation (1).

Notice that the two angles, (θ_1, θ_2), can be different from each other and their values can be changed, at segmentation step, to detect each pupil and iris boundaries; we made automatic segmentation by using a single value for the Ubiris and another one for the Upol database.

The iris segmentation step in the Ubiris database is particularly challenging due to the presence of partially occluded irises, as shown in figure 2:

Fig. 2. Partially occluded iris in the Ubiris database.

That is, the Ubiris database stores eyes where the eyelid covers most of the iris; obviously, in such a case, the iris segmentation step fails and the identification process ends in misclassification. In our experiments we did not choose the images to work with, and, therefore, we used also these partially (totally) occluded irises, which, obviously, contributed to the error rate. That is, when all images of the Ubiris database are used, the minimum error rate must be set to the number of close eyes over the total number of images.

The particularity of the Upol [22] database is that the eye is photographed through a black hole, which results in a black circle outside the sclera. To segment the Upol database we used the variation of equation (1) proposed by Hebaishy, [23]: while searching for the limbus by increasing the radius r, the detected outer circle is the first one having an integro-differential value

biggest that the threshold. Figure 3 shows some irises of the Upol database: the 1st row stores the original pictures, the 2nd row zooms on the corresponding problematic areas. Moreover, while all irises have the black frame outside the sclera, some cases are more challenging because of (1) the presence of a white circle inside the pupil (due to the reflection of the camera) and/or (2) blurred boundaries.

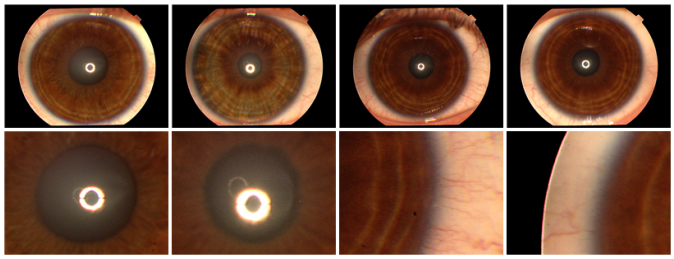

Fig. 3. 1st row: challenging irises in the Upol database, 2nd row: zoom on the corresponding problematic areas.

To summarize, we point out that the segmentation of Upol images was more challenging than the one of Ubiris database mainly due to the circular black mask around the captured iris image. Figure 4 shows segmented iris images from the Ubiris and the Upol databases:

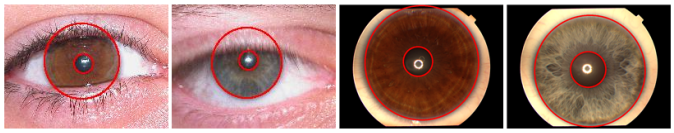

Fig. 4. Segmented iris sample from the Ubiris (2 pictures on the left) and the Upol (2 eyes on the right) databases.

B. Angular Radial Partitioning

The Angular Radial Partitioning (ARP) method [14] is a common used technique for edge detection; the main objective of ARP is to re-write the original image into a new structure, which must be is invariant to scale and rotation, while being capable of supporting measurement of similarity between images. In [16] Celebi used ARP for texture based iris recognition systems. We followed his example and we used ARP to partition the segmented iris region into a number of sectors. More in details:

1. The iris texture is converted from Cartesian to polar coordinate axes; that is $Iris(x, y)$ becomes $I(\rho, \theta)$, and we adopted the convention to indicate with $I(\rho, \theta)$ also the greylevel of the pixel in position (ρ, θ);

2. The radius of the iris, R, is divided into M radial partitions and the circle angle, $\theta = 360°$, is partitioned into N angular sub-angles, which resulted in a $M \times N$ sectors.

Figure 5 illustrates this concept in case of $\theta = 180°$ angle.

After ARP segmentation, the iris image is divided into a set of sectors, $\{sector(k, i)\}$ for all $k = 0, ..., M-1$ and $i = 0, ..., N-1$. In equation 2:

$$Iris = \{sector(k, i)\} = \sum_{\rho=\frac{kR}{M}}^{\frac{(k+1)R}{M}} \sum_{\theta=\frac{i2\pi}{N}}^{\frac{(i+1)2\pi}{N}} I(\rho, \theta) \qquad (2)$$

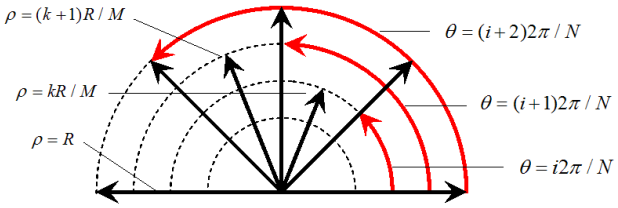

Fig. 5. Angular Radial Partitioning(ARP) with M radial partitions and N angular partitions.

Very often the papillary and limbus circles are not concentric, that is the pupil centre is different from the iris one. ARP uses the pupil circle centre coordinates to make segmentation; if iris coordinates were used, partitions could slide bringing to worse classification results.

The proposed system does not use first and last radial partitions, because they could contain the data from the pupil's texture or the one form the sclera; this expedient reduces the total complexity of the system and it has also the advantage to limit the misclassification effect, due to the presence of eyelashes and eyelids around the upper/lower limbus's areas. As a result, the total number of acquired segment is $(M-2) \times N$.

Figure 6 shows the results of ARP segmentation on Ubiris and Upol databases; the picture has been produced by working with the iris image $I(\rho, \theta)$ and increasing the values of ρ and θ so as to cover all iris; the outer and inner sectors will not be considered.

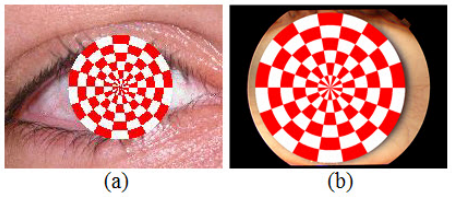

Fig. 6. Results of the Angular Radial Partitioning on Ubiris (a) and Upol (b) image samples.

III. Feature Extraction

A. Sum & Difference Histograms (SDH)

The method used for texture analysis is the Sum and Difference Histogram (SDH) algorithm introduced by Unser in [15] and used for (marble) texture analysis by Alajardin et al. [24]. SDH is an alternative to the Grey-level Co-occurrence Matrices (GLCM) method [25]; it has the big advantage of decreasing both memory storage and computational time while keeping similar performance. Representing a texture of a greyscale image with SDH technique requires the calculation of the sum and difference vectors, with the corresponding normalized sum and difference histograms. Let us consider a $K \times L$ b-bit grey-level picture having $N_G = 2^b$ quantized grey-levels, e.g. in case of $b = 8$ $N_G = 256$, and the range (R) of intensity greylevel values $R_{greylevel} = [0, \ldots, N_G - 1]$; finally, let us define as $y_{k,l}$ the grey-level of the pixel in position (k, l), for $k = 1, \ldots, K$ and $l = 1, \ldots, L$. With SDH, out of its 8 neighbours, for every pixel, we are interested only in the four pixels situated in non-opposite directions, that

is $D = \{(-1,-1),(-1,0),(-1,1),(0,1)\}$. Figure 7 shows the 8-Neighborhood of a texture pixel and names the four neighbour pixels used by the Sum and Difference Histogram (SDH): $\{V_1, V_2, V_3, V_4\}$; adopting the same convention as before, the position of the pixel gives also its greylevel values; that is, V_1 is the name of the top-left pixel of $y_{k,l}$, the centre pixel $(*)$, and it is also its greylevel value.

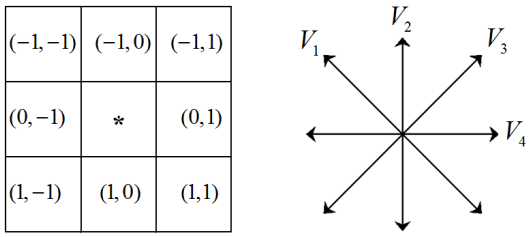

Fig. 7. 8-Neighborhood of a texture pixel and the four neighbourhood directions used by SDH algorithm.

Still considering the $K \times L$ b-bit grey-level picture, we calculate the sum and the difference vectors using equation (3) and (4) by moving the centre pixel, $y_{k,l}$, starting from the bottom-left corner of the image and ignoring the top row and the most right column of the picture, that is, for all $l = 1,\ldots,L-1$ and $k = 1,\ldots,K-1$:

$$sum_{k,l} = y_{k,l} + (V_1 + V_2 + V_3 + V_4)/4 \quad (3)$$

$$diff_{k,l} = y_{k,l} - (V_1 + V_2 + V_3 + V_4)/4 \quad (4)$$

In words, the sum (difference) vector stores the sum (minus) of the greylevel of pixel (k,l) with the average greylevels of the fours neighbours of $y_{k,l}$. The resulting size of both vectors, $sum_{k,l}$ and $diff_{k,l}$, is therefore $(K-1)\times(L-1)$, and the range of their intensity grey-levels is, respectively, $R_{sum} = [0,\ldots,2*(N_G-1)]$ and $R_{diff} = [-(N_G-1),\ldots,N_G-1]$. In case of 8-bit picture, $R_{greylevel} = [0,\ldots,255]$, the range of the sum vector is $R_{sum} = [0,\ldots,510]$ and the range of the difference vector is $R_{diff} = [-255,\ldots,255]$. In this work, we applied the SDH technique sector wise; that is, for every sector, we calculated the couple $(sum_{k,l}, diff_{k,l})$ vector, starting from the smallest values of ρ and θ and increasing by '1', either pixel or degree, at every step. Notice that for little circle, $\rho = 1$, the increase of $\theta = 1^\circ$ can result in the same pixel in the Cartesian coordinate; when this happens we increased again the angle θ. That is, because the shape of a sector is not square, we searched for the next centre pixel $y_{k,l}$ and for its neighbours $\{V_1, V_2, V_3, V_4\}$ using polar coordinates and increasing either ρ or θ; the resulting pixel's position is then mapped into Cartesian coordinate and duplicated pixels are ignored. The size of both vectors, $sum_{k,l}$ and $diff_{k,l}$, changes depending to the sector's size, but the range of their intensity grey-levels is fixed to $R_{sum} = [0,\ldots,2*(N_G-1)]$ and $R_{diff} = [-(N_G-1),\ldots,N_G-1]$. The histograms of the sum and the difference vectors are calculated using equations (5) and (6), sector wise:

$$h_{sum}(i) = Card\{(k,l) \in sector, sum_{k,l} = i\} \quad for\ all\ i = 0,\ldots,2*(N_G-1) \quad (5)$$

$$h_{diff}(j) = Card\{(k,l) \in sector, diff_{k,l} = j\} \quad for\ all\ j = -N_G-1,\ldots,N_G-1 \quad (6)$$

where "$Card$" is the total number of pixel having greylevel value "i" in the considered sector. Knowing $SectPixel = \sum_i h_{sum}(i) = \sum_j h_{diff}(j)$, the total number of pixels in the actual sector, the normalized sum and difference histogram vectors are the corresponding probability vectors:

$$P_{sum}(i) = h_{sum}(i)/SectPixel \quad (7)$$

$$P_{diff}(j) = h_{diff}(j)/SectPixel \quad (8)$$

Notice that the size of all histograms and probability vectors is fixed to $2*(N_G-1)$; that is, their dimension is independent to the sectors's size. When the input picture is a colourful one SDH calculates three sum and three difference vectors, one for each colour channels, and converts them into three couples of probability vectors, $(P_{sum}(i), P_{diff}(j))$. Interesting to point out that, the memory requirement of SDH is always better that the one of the GLCM method; that is, in case of RGB image, GLCM makes texture analysis considering the 8-Neighbours of the centre pixel, $y_{k,l}$, by building and processing 3 matrices of size $N_G \times N_G$. For example, in case of a 8-bit RGB image, the memory requirement of SDH is $3 \times 2 \times 2 \times (N_G-1) = 3060$ elements (3 for the palettes, R,G,B; 2 for the sum and difference vectors; $2\times(N_G-1)$ is the fix size of every probability vector), while GLCM requires $3 \times N_G \times N_G = 196608$ elements.

B. Statistical Features from Texture

Seven statistical features are calculated out of the two SDH vectors of every ARP sector, namely: mean, variance, energy, correlation, entropy, contrast and homogeneity features. Table I gives their formulas.

TABLE I. FORMULAS TO CALCULATE THE STATISTICAL PARAMETERS

Parameter	**Formulas**
Mean	$\frac{1}{2}\sum_i i \cdot P_s(i) = \mu$
Variance	$\frac{1}{2}(\sum_i (i-2\mu)^2 \cdot P_s(i) + \sum_j j^2 \cdot P_d(j))$
Energy	$\sum_i P_s(i)^2 \cdot \sum_j P_d(j)^2$
Correlation	$\frac{1}{2}(\sum_i (i-2\mu)^2 P_s(i) - \sum_j j^2 \cdot P_d(j))$
Entropy	$-\sum_i P_s(i)\cdot \log P_s(i) - \sum_j P_d(j)\cdot \log P_d(j)$
Contrast	$\sum_j j^2 \cdot P_d(j)$
Homogeneity	$\sum_j \frac{1}{1+j^2} \cdot P_d(j)$

Interesting to notice that ARP sectors with different radial distance from the centre have a variable number of pixels; out of every sector the SDH algorithm calculates two fix size vectors, (P_{sum}, P_{diff}), which are then converted into seven features. In other words, sectors of different sizes contribute with fix size feature vectors.

The length of the extracted feature vectors depends to the type of the processed image: ranging from $(M-2)\times N \times 7$ in case of greyscale picture to $(M-2)\times N \times 7 \times 3$ for RGB images. In the specific case of $M = 6$ and $N = 18$, with

a 24-bits colour image, the resulting feature vector has size $(6-2) \times 18 \times 7 \times 3 = 1512$. As ARP partition counts were decreased, feature vector length became shorter.

IV. Experiments and Results

We evaluated the performance of the proposed texture-based iris recognition system on two different databases; we chose the Ubiris and the Upol databases since they are both challenging databases and have different disturbance elements; that is, while in the Ubiris database the main issues are illumination and partial occlusion, in the Upol database problematic pictures have a white circle inside the pupil, due to reflection of the camera, and/or blurred limbus contour.

The Ubiris [21] database includes 1877 images captured from 241 people in two sessions using a Nikon E5700 model camera; pictures capture in first session have less noise comparing with the ones of the second session. Images have resolution of 150×200 pixels and are either 24-bits RGB or greyscales. Ubiris is known as a challenging iris database due to poor focus of the images and the presence of reflection and partial occlusion of the iris; some statistics are shown in table II.

TABLE II. Ubiris database characteristics with classification parameters [26].

Percantages	Good	Average	Bad
Focus	73.83 %	17.53 %	8.63 %
Reflections	58.87 %	36.78 %	4.34 %
Visible Iris	36.73 %	47.83 %	15.44 %

Out of every subject we selected the first five pictures, with the only exception of one person who has only four iris images. That is, we did not choose good irises nor discard problematic images, and we used both greyscale and RGB irises; this selection process results in $5 \times 241 - 1 = 1204$ images. We pre-processed the images with the MATLAB library function "imfill" to clear the original samples from light reflections on iris and pupil regions, as shown in Figure 8:

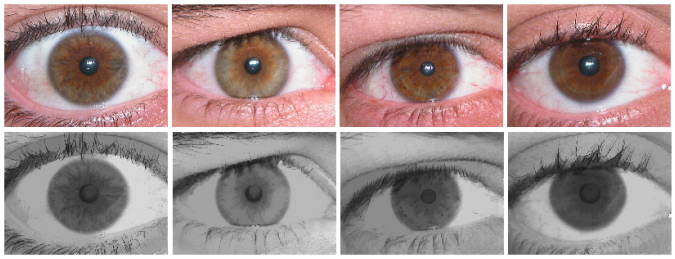

Fig. 8. Original Ubiris images (1st row) versus pre-processed ones (2nd row).

The Upol [22] iris database stores $128 \times 3 = 384$ images captured from right and left eyes of 64 people's. Images are 24 bits, have resolution 576×768 pixels and were taken with SONY DXC-950P 3CCD camera. The main challenges of the Upol database are (1) the black frame surrounding the sclera, due to the particular process used to take the images, (2) the presence of a white circle inside the pupil, due to the reflection of the camera, and (3) a blurred limbus, the outer circle of the iris. We worked with all images.

In all experiments we worked in a close environment, where the input test sample belongs to one of the training subject. To maximize the amount of training and testing data, we made classification using the k-fold cross validation technique: at the first round, the test set is made up of all first instances of every class, which are classified using all remaining samples as training images; the same process is repeated with the second, third, ..., and $m-th$ instance.

In case of the Upol database, having 64 subjects and $64 \times 2 = 128$ classes, $n = 128$ and $m = 3$, while the Ubiris database has $n = 241$ classes and $m = 5$ samples per class; it follows that the k-fold cross validation technique has $k = 3$, when working with the Upol database, and $k = 5$, when working with the Ubiris database.

We run our experiments in the identification mode (one-to-many matching) and we evaluated the performance of our system using the Correct Recognition Rate (CRR), which is the percentage of correct classified irises out the total number of test sample. We compared classification performances of K-NN. Following the study of Celebi, [16], we fixed $N = 18$ and we run different experiments ranging M in $[6, 8, 10, 12, 20]$; classification results are stored in the following tables:

TABLE III. CRR (%) on Ubiris grey images for different values of M (parameter of ARP) and distances.

MxN:ARP Parameters	6x18	8x18	10x18	12x18	20x18
K-NN (Euclidean)	93.52	94.85	94.68	94.93	94.60
K-NN (Manhattan)	95.68	95.76	95.93	96.01	95.84

TABLE IV. CRR (%) on Ubiris color images for different values of M (parameter of ARP) and distances.

MxN:ARP Parameters	6x18	8x18	10x18	12x18	20x18
K-NN (Euclidean)	94.85	95.01	95.26	95.68	94.68
K-NN (Manhattan)	95.84	96.09	96.17	96.51	95,68

TABLE V. CRR (%) on Upol grey images for different values of M (parameter of ARP) and distances.

MxN:ARP Parameters	6x18	8x18	10x18	12x18	20x18
K-NN (Euclidean)	94.27	94.53	95.31	95.83	95.83
K-NN (Manhattan)	96.09	95.83	96.35	96.87	96.87

TABLE VI. CRR (%) on Upol color images for different values of M (parameter of ARP) and distances.

MxN:ARP Parameters	6x18	8x18	10x18	12x18	20x18
K-NN (Euclidean)	95.31	95.05	95.31	96.35	95.57
K-NN (Manhattan)	96.35	97.39	96.87	97.39	96.87

Results of Tables III-VI show that the best performance is reached with $M = 12$ and K-NN using the Manhattan distance.

Having "n" classes, we created a Confusion Matrix, CM, of size $n \times n$, where rows label the actual class and columns the predicted class. The initial values of $CM(i,j) = 0$, for all $i = 1, \ldots, n$ and $j = 1, \ldots, n$, and $CM(i,j)$ is increased by "1" whenever a sample of $class_i$ is assigned to $class_j$; ideally, CM is a diagonal matrix with all off-diagonal elements equal to "0" and $C(i,i)$ is equal to the total number of samples belonging to $class_i$. When classification errors occur, $C(i,j)$

is equal to the number of samples belonging to $class_i$ and assigned to $class_j$, $i \neq j$.

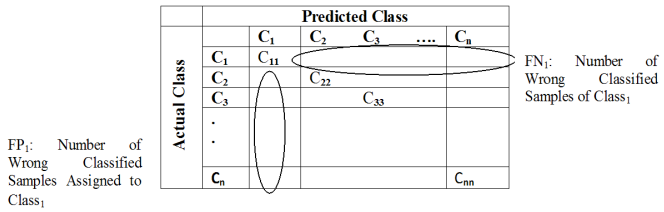

Fig. 9. The Class Confusion Matrix.

The following equations define (9) the False Positive of $class_i$, FP_i; which is equal to the sum of off-diagonal elements of $column(i)$; (10) the False Acceptance Rate of $class_i$, FAR_i; (11) the weight of $class_i$, W_i; (12) the False Acceptance Rate, FAR; which is equal to the weighted sum of FAR_i; (13) the False Negative of $class_i$, FN_i; which is equal to the sum of off-diagonal elements of $row(i)$; (14) the False Rejection Rate of $class_i$, FRR_i; and (15) the False Rejection Rate; in all equations "$Number\ Sample_i$" stands for the number of samples belonging to $class_i$:

$$FP_i = Number\ of\ Wrong\ Classified\ Sample_j \\ Assigned\ to\ Class_i \quad (9)$$

$$FAR_i = \frac{FP_i}{(Total\ Num.\ Sample - Num.\ Sample_i)} \quad (10)$$

$$W_i = \frac{Number\ Sample_i}{Total\ Number\ Sample} \quad (11)$$

$$FAR = \sum_{i=1}^{n} FAR_i \cdot W_i \quad (12)$$

$$FN_i = Number\ of\ Sample_i\ Wrongly \\ Assigned\ to\ Class_j \quad (13)$$

$$FRR_i = \frac{FN_i}{Number\ Sample_i} \quad (14)$$

$$FRR = \sum_{i=1}^{n} FRR_i \cdot W_i \quad (15)$$

Notice that, in case of the Upol and Ubiris databases, all weights are equal because all classes have the same number of samples.

In the following table we report the values of FAR and FRR in case of K-NN with the Manhattan distance and $M \times N = 12 \times 18$ ARP sectors:

Interesting to notice that the low value of FAR is due to the very good performance of the proposed system but also to the characteristics of our experiments, having only one test sample per class and a high number of classes.

Figure 10 stores some of the misclassified irises belonging to the Ubiris database. In this study, we did not choose the pictures to work with, and figure 10 shows that misclassification occurs for occluded irises, practically impossible to be recognized; that is, considering that 15.44% of the irises are not visible, our average CRR of 96.5% is virtually equivalent to the best possible performance.

TABLE VII. PERFORMANCE MEASUREMENTS (%) OF THE PROPOSED TEXTURE BASED IRIS IDENTIFICATION SYSTEM.

Database	Color Format	FAR	FRR
Ubiris	grey	0.02	3.99
	color	0.01	3.49
Upol	grey	0.03	3.12
	color	0.02	2.60

Fig. 10. Misclassified irises in the Ubiris database.

With the aim to investigate on the correlation between segmentation and classification steps, we report in table VIII the average segmentation accuracy on both databases:

TABLE VIII. AVERAGE SEGMENTATION ACCURACY ON THE UBIRIS AND UPOL DATABASES.

Dataset	Accuracy (%)
Ubiris	97
Upol	83

Comparing these results with the CRR of table VII, we may say that, in case of the Ubiris database, the majority of the error is due to mis-segmentation; that is, we segmented in a correct way 97% of the eyes, and we classify in a proper way 96% of them; the 1% difference is due to added classification error. On the contrary, in case of the Upol database, only 83% of the images are segmented in a correct way, .but still the average CRR is 96%; that is, the sub-sequent classification step can recover for little shifts in segmentation boundary, and this is due, mainly, to the high resolution of the irises. Figure 11 stores some of the mis-segmented irises belonging to the Upol database, only the last two were mis-classified:

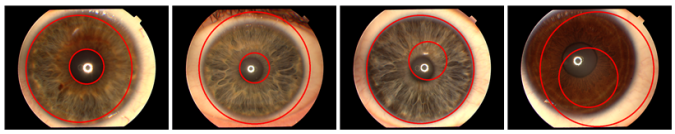

Fig. 11. Mis-segmented irises in the Upol database.

One of the main problems encountered during this work was to find a benchmark paper storing a clear description of the experiments run, so as to be able to reproduce them and compare the resulting performances. We chose the two papers of Celebi [16] and Erbilek et al. [17] because we were attracted by their algorithms and they have a partial description of the experiments. That is, like Celebi and Erbilek, we worked with the Ubiris and Upol databases in identification mode (one-to-many matching); unfortunately, in case of the Ubiris database, [16] does not give any other information, neither the section of the used images, which remains undefined; while [17] used

images of section 1, they selected 80 subjects to work with (but we do not know which subjects), and they manually cropped all irises. Table IX stores a comparison of the results of these three systems:

TABLE IX. UBIRIS DATABASE: CRR (%) COMPARISON OF DIFFERENT IRIS BASED RECOGNITION SYSTEMS.

	Celebi [16]	**Erbilek [17]**	**Proposed**
Session	Not known	Session 1	Session 1
CRR	94.44	95.83	96.51

In case of [16], not knowing the session of the used images, it is possible to make only a mild comparison on the CRR. On the contrary, comparing the performance of the proposed system with the one of Erbilek et al., we point out that we reached better results also by selecting the first five images of all subjects and by using automatic segmentation of the irises. That is, CRR values together with the random selections of the images and the automatic segmentation of the irises make our system superior to the one of [17]. Experiments on the Upol database are too obscured to be compared.

V. CONCLUSIONS

In the proposed texture based iris recognition system, (1) we made automatic segmentation of the iris using a variation of the Daugman's integro-differential operator followed by the ARP technique, which is invariant to scale and rotation; (2) we did not use the first and last radial partition, because they could contain eyelids and eyelashes as well as data from the pupil's and sclera's texture; (3) we extracted seven dimensional feature out of every sector by re-writing the sector's texture into two probability vectors.

Our experiments indicate that this new system has the advantage to be robust to a wide variety of disturbance elements, such as partial occlusion of the iris, poor focus of the image, illumination effects and blurred contours. Moreover, the low percentage of FAR obtained in out trails suggests that the proposed approach is a good prototype for biometric recognition systems run in identification mode, where security is a key issue. Another important advantage of this new approach is the little number of samples per class necessary to train it; that is, while in the Ubiris database we worked with 241 classes and we used only 4 training samples per class, in the Upol database 2 training samples per class are enough to identify a person out of 128 classes, 97% of the time.

REFERENCES

[1] J. Daugman, "High confidence visual recognition of persons by a test of statistical independence," *IEEE Transactions on Pattern Analysis and Machine Intelligence*, vol. 15, no. 11, pp. 1148–1161, Nov. 1993.

[2] J. Daugman, "The importance of being random: statistical principles of iris recognition," *Pattern Recognition*, vol. 36, no. 2, pp. 279–291, Feb. 2003.

[3] J. Daugman, "How iris recognition works," *IEEE Transactions on Circuits and Systems for Video Tech.*, vol. 14, no. 1, pp. 21–30, Jan. 2004.

[4] R. Wildes, J. Asmuth, G. Green, S. Hsu, R. Kolczynski, and S. McBride, "A system for automated iris recognition," in *Proceedings of the Second IEEE Workshop on Applications of Computer Vision*, Sarasota, FL, Dec. 5–7, 1994, pp. 121–128.

[5] P. Belhumeur, J. Hespanha, and D. Kriegman, "Eigenfaces vs fisherfaces: recognition using class specific linear projection," *IEEE Transactions on Pattern analysis and Machine Intelligence*, vol. 19, no. 7, pp. 711–720, Jul. 1997.

[6] W. Boles and B. Boashash, "A human identification technique using image of the iris and wavelet transform," *IEEE Transactions on Signal Processing*, vol. 46, no. 4, pp. 1185–1188, Apr. 1998.

[7] L. Ma, T. Tan, Y. Wang, and D. Zhang, "Local intensity variation analysis for iris recognition," *Pattern Recognition*, vol. 37, no. 6, pp. 1287–1298, Jun. 2004.

[8] K. Bowyer, K. Hollingsworth, and P. Flynn, "Image understanding for iris biometrics: a survey," *Computer Vision and Image Understanding*, vol. 110, no. 2, pp. 281–307, May 2008.

[9] C. Chen and C. Chu, "High performance iris recognition based on 1-d circular feature extraction and pso–pnn classifier," *Expert Systems with Applications*, vol. 36, no. 7, pp. 10 351–10 356, Sep. 2009.

[10] F. Sibai, H. Hosani, R. Naqbi, S. Dhanhani, and S. Shehhi, "Iris recognition using artificial neural networks," *Expert Systems with Applications*, vol. 38, no. 5, pp. 5940–5946, May 2011.

[11] J. Pillai, V. Patel, R. Chellappa, and N. Ratha, "Secure and robust iris recognition using random projections and sparse representations," *IEEE Transactions on Pattern Analysis and Machine Intelligence*, vol. 33, no. 9, pp. 1877–1893, Sep. 2011.

[12] Y. Si, J. Mei, and H. Gao, "Novel approach to improve robustness, accuracy and rapidity of iris recognition systems," *IEEE Transactions on Industrial Informatics*, vol. 8, no. 1, pp. 110–117, Feb. 2012.

[13] A. Rahulkar and R. Holambe, "Half-iris feature extraction and recognition using a new class of biorthogonal triplet half-band filter bank and flexible k-out-of n: a post-classifier," *IEEE Transactions on Information Forensics and Security*, vol. 7, no. 1, pp. 230–240, Feb. 2012.

[14] A. Chalachale, A. Mertins, and G. Naghdy, "Edge image description using angular radial partitioning," *IEEE Proceedings on Vision, Image and Signal Processing*, vol. 151, no. 2, pp. 93–101, Apr. 2004.

[15] M. Unser, "Sum and difference histograms for texture classification," *IEEE Transactions on Pattern Analysis and Machine Intelligence*, vol. 8, no. 1, pp. 118–125, Jan. 1986.

[16] A. Celebi, M. Gullu, and S. Erturk, "Low–complexity iris recognition using one-bit transform and angular radial partitioning," in *IEEE Signal Processing and Communications Applications Conference (SIU)*, Antalya, Apr. 2009, pp. 696–699.

[17] M. Erbilek and O. Toygar, "Recognizing partially occluded irises using sub-pattern-based approaches," in *International Symposium on Computer and Information Sciences (ISCIS)*, Guzelyurt, Sep. 2009, pp. 606–610.

[18] J. Canny, "A computational approach to edge detection," *IEEE Transactions on Pattern Analysis and Machine Intelligence*, vol. 8, no. 6, pp. 679–698, Nov. 1986.

[19] Y. Jang, B. Kang, and K. Park, "A study on eyelid localization considering image focus for iris recognition," *Pattern Recognition Letters*, vol. 29, no. 11, pp. 1698–1704, Aug. 2008.

[20] T. Tan, Z. He, and Z. Sun, "Efficient and robust segmentation of noisy iris images for non-cooperative iris recognition," *Image and Vision Computing*, vol. 28, no. 2, pp. 223–230, Feb. 2010.

[21] H. Proenca and L. Alexandre. Ubiris iris image database: http://iris.di.ubi.pt.

[22] M. Dobes and L. Machala. Upol iris image database: http://phoenix.inf.upol.cz/iris/.

[23] M. Hebaishy. Poster: Optimized daugman's algorithm for iris localization, http://wscg.zcu.cz/wscg2008/papers_2008/poster/a11–full.pdf.

[24] J. Alajarin, J. Luis-Delgado, and L. Tomas-Balibrea, "Automatic system for quality-based classification of marble textures," *IEEE Transactions on Systems, Man and Cybernetics-Part C: Applications and Reviews*, vol. 35, no. 4, pp. 488–497, Nov. 2005.

[25] R. Gonzales and R. Woods, Eds., *Digital Image Processing*. 3th Pearson Int. Edition, 2008.

[26] Ubiris classification statistics, http://iris.di.ubi.pt/ubiris1.html.

[27] C. Burges, "A tutorial on support vector machines for pattern recognition," *Data Mining and Knowledge Discovery*, vol. 2, no. 2, pp. 121–167, 1998.